Biogeosciences Discuss., 5, 2867–2896, 2008
www.biogeosciences-discuss.net/5/2867/2008/

Biogeosciences Discussions

Biogeosciences Discussions is the access reviewed discussion forum of *Biogeosciences*

Anthropogenic and biophysical contributions to increasing atmospheric CO_2 growth rate and airborne fraction

M. R. Raupach[1], **J. G. Canadell**[1], **and C. Le Quéré**[2,3]

[1]Global Carbon Project, CSIRO Marine and Atmospheric Research, Canberra, Australia
[2]School of Environmental Sciences, University of East Anglia, Norwich, UK
[3]British Antarctic Survey, Cambridge, UK

Received: 2 June 2008 – Accepted: 4 June 2008 – Published: 11 July 2008

Correspondence to: M. R. Raupach (michael.raupach@csiro.au)

Published by Copernicus Publications on behalf of the European Geosciences Union.

Abstract

We quantify the relative roles of natural and anthropogenic influences on the growth rate of atmospheric CO_2 and the CO_2 airborne fraction, considering both interdecadal trends and interannual variability. A combined ENSO-Volcanic Index (EVI) relates most (~75%) of the interannual variability in CO_2 growth rate to the El-Niño-Southern-Oscillation (ENSO) climate mode and volcanic activity. Analysis of several CO_2 data sets with removal of the EVI-correlated component confirms a previous finding of a detectable increasing trend in CO_2 airborne fraction (defined using total anthropogenic emissions including fossil fuels and land use change) over the period 1959–2006, at a proportional growth rate 0.24% y^{-1} with probability ~0.9 of a positive trend. This implies that the atmospheric CO_2 growth rate increased slightly faster than total anthropogenic CO_2 emissions. An extended form of the Kaya identity relates the increase in the CO_2 growth rate (1.9% y^{-1} over 1959–2006) to the growth rates of four global driving factors: population (contributing +1.7% y^{-1}); per capita income (+1.8% y^{-1}); the total carbon intensity of the global economy (−1.7% y^{-1}); and airborne fraction (averaging +0.2% y^{-1} with strong interannual variability). Together, the recent (post-2000) increase in growth of per capita income and decline in the negative growth (improvement) in the carbon intensity of the economy will drive a significant acceleration in the CO_2 growth rate over coming decades, unless these recent trends reverse. To achieve an annual reduction rate in total emissions of −2% y^{-1} (which would halve emissions in 35 years) in the presence of a per-capita income growth rate of 2% y^{-1} and a population growth rate of 1% y^{-1}, it is necessary to achieve a decline in total carbon intensity of the economy at a rate of around −5% y^{-1}, three times the 1959–2006 average.

1 Introduction

Atmospheric CO_2 concentrations have risen over the last 200 years at an accelerating rate, in response to increasing anthropogenic CO_2 emissions. The resulting CO_2 dise-

quilibrium has led to uptake of CO_2 from the atmosphere by land and ocean CO_2 sinks, which currently remove over half of all anthropogenic emissions and thereby provide a strong negative (stabilising) feedback on the carbon-climate system (Gruber et al., 2004; Sabine et al., 2004). The CO_2 airborne fraction (the fraction of total emissions from fossil fuels and land use change accumulating in the atmosphere) has averaged 0.43 since 1959, but has increased through that period at about 0.24% y^{-1} (Canadell et al., 2007). These interdecadal trends in CO_2 growth rate and the airborne fraction are the outcome of a race between two groups of forcing factors: the social, economic and technical drivers of anthropogenic emissions (including population, wealth and the carbon intensity of the economy), and the biophysical drivers of trends in land and ocean sinks.

The CO_2 growth rate also varies strongly at interannual (~1 to ~10 y) time scales, through mainly biophysical mechanisms. Fluctuations in CO_2 growth rate correlate with the El-Niño-Southern-Oscillation (ENSO) climate mode (Keeling and Revelle, 1985; Keeling et al., 1995; Jones and Cox, 2005), because the terrestrial carbon balance in tropical regions is tilted from uptake to release of CO_2 during dry, warm El-Niño events (Zeng et al., 2005; Knorr et al., 2005). Volcanic events are also significant: the CO_2 growth rate decreased for several years after the eruption of Mt. Pinatubo in June 1991 (Jones et al., 2001), probably because of increased net carbon uptake by terrestrial ecosystems due to higher diffuse solar radiation (Gu et al., 2003) and cooler temperatures (Jones and Cox, 2001) caused by volcanic aerosols. This interannual variability in the CO_2 growth rate is important for two reasons: it indicates mechanisms that govern the land and ocean CO_2 sinks, and it masks important longer-term trends in the CO_2 growth rate with strong variability at higher frequencies.

In this paper we investigate the combined anthropogenic and biophysical drivers of atmospheric CO_2 growth rates, with three aims. First, we obtain a simple quantification of the leverage of ENSO and volcanic signals on global CO_2 sinks at interannual time scales, using a combined ENSO-Volcanic Index (EVI). Second, we analyse observed interdecadal trends in the CO_2 airborne fraction by removing the interannual variabil-

ity associated with the EVI from several CO_2 records, confirming and extending the preliminary findings of Canadell et al. (2007). Third, we introduce an extended form of the Kaya identity which combines the biophysical and anthropogenic drivers of CO_2 growth, and use it both to diagnose the drivers of past trends and offer some indicative estimates of future CO_2 growth rates.

2 Framework

2.1 Atmospheric CO_2 budget and airborne fraction

The global atmospheric CO_2 budget is written as

$$C'_a = F_E + F_S = (F_{\text{Foss}} + F_{\text{LUC}}) + (F_{\text{LandAir}} + F_{\text{OceanAir}}) \quad (1)$$

where $C_a = v_a[CO_2]$ is the mass of atmospheric CO_2 (with $[CO_2]$ the atmospheric CO_2 mole fraction and $v_a = 2.127$ PgC ppm^{-1}); $C'_a = dC_a/dt$ is the growth rate of atmospheric CO_2 (with primes denoting time derivatives); F_E is the total anthropogenic CO_2 emission flux including emissions from fossil fuels (F_{Foss}) and net emissions from land use change (F_{LUC}); and F_S is the total surface-air exchange flux including land-air and ocean-air fluxes (F_{LandAir} and F_{OceanAir}). All fluxes are positive into the atmosphere, so $F_S < 0$ in the current era and the total CO_2 sink is $-F_S$.

The CO_2 airborne fraction, the fraction of emissions accumulating in the atmosphere, has two extant definitions based respectively on total anthropogenic emissions from both fossil fuels and land use change ($F_E = F_{\text{Foss}} + F_{\text{LUC}}$), and on fossil-fuel emissions only (F_{Foss}):

$$a_E = C'_a/F_E; \quad a_{\text{Foss}} = C'_a/F_{\text{Foss}} \quad (2)$$

where the subscript denotes the normalising flux. The former (a_E) is the "total" airborne fraction, while the latter (a_{Foss}) has been called the "apparent" airborne fraction (Oeschger et al., 1980; Enting, 2007). Similarly, a sink fraction (the fraction of

emissions taken up by land and ocean sinks, $-F_S$) can be defined in two ways as $s_E = -F_S/F_E$ (total) and $s_{\text{Foss}} = -F_S/F_{\text{Foss}}$ (apparent). The relationships between the respective airborne and sink fractions are

$$a_E = 1 - s_E; \quad a_{\text{Foss}} = 1 - s_{\text{Foss}} + (F_{\text{LUC}}/F_{\text{Foss}}) \tag{3}$$

The total airborne fraction a_E is preferable in principle to the apparent a_{Foss}, for two reasons. First, a_E is the ratio of total response of the atmospheric carbon cycle (C'_a) to total forcing (F_E), whereas a_{Foss} is the ratio of total response (C'_a) to a partial forcing (F_{Foss}), omitting F_{LUC}. Second (and in consequence), the total airborne and sink fractions add to 1, so trends in a_E are always opposite to trends in s_E and either fraction is a direct measure of the outcome of the combined influences of total emissions and total sinks on the CO_2 growth rate. The apparent airborne and sink fractions do not have this property because the additional forcing from land use change has to be included separately (Eq. 3).

Longstanding use of the apparent airborne fraction was originally motivated not from basic considerations but by the methodological problem of lack of knowledge of F_{LUC}. However, the situation has now changed with improved data, especially from satellites. Recent estimates of F_{LUC} have converged on 1.5±0.5 PgC y^{-1} for 2000–2006, compared with $F_{\text{Foss}} \approx 7.6 \pm 0.4$ and $C_a{}' \approx 4.1 \pm 0.1$ PgC y^{-1} over the same period (Canadell et al., 2007).

In this paper a_E is used as the primary measure of airborne fraction, but results are also given for a_{Foss}.

2.2 Data

We used the following data for the period 1959 to 2006 (see Appendix A for sources and details):

– annual global CO_2 emissions F_{Foss} and F_{LUC};

- monthly CO_2 series with the annual cycle removed, from atmospheric baseline stations at Mauna Loa, Hawaii (MLO) and the South Pole (SPO), together with two estimates of globally averaged CO_2 concentration: the first (GLA) was formed from the average of MLO and SPO, and the second (GLB) consisted of a globally-averaged CO_2 series available from January 1980 onward, augmented with MLO data for 1958–1979;
- five monthly ENSO indices: eastern (Niño3), central (Niño3.4) and western (Niño4) equatorial Pacific sea surface temperatures, the Southern Oscillation Index (SOI), and the Multivariate ENSO Index (MEI);
- the monthly global Volcanic Aerosol Index (VAI);
- global population and Gross Domestic Product by Purchasing Power Parity (GDP-PPP).

The analysis was done at a monthly time step, with slowly varying annual data (emissions, population, GDP-PPP) interpolated to monthly (details in Appendix A).

3 Interannual variability of CO_2 growth rate

3.1 Spectral structure of CO_2 growth and ENSO

Figure 1 shows normalised cumulative spectra and cospectra of the CO_2 growth rate and each of the five ENSO indices (Niño3, Niño3.4, Niño4, SOI, and MEI). Normalised (co)spectra show the fractional contribution to the (co)variance from frequencies less than a given frequency (see Appendix B for analytical details). All of the covariance between C'_a and any of the five ENSO indices is spectrally band-limited to frequencies in a narrow window between ~0.2 and ~0.8 y^{-1} (periods from ~5 to ~1.25 y). Spectral components of C'_a and ENSO indices at higher frequencies add nothing to the covariance, their only effect being to degrade the correlation by adding uncorrelated

high-frequency noise. It is therefore useful to filter out the high-frequency noise for diagnosis of the relationship between ENSO and carbon fluxes. Henceforth all time series are lowpass-filtered with a Fourier-transform filter which removes frequencies $f > 0.8\,\mathrm{y}^{-1}$ or periods <15 months (see Appendix B for details).

3.2 Correlations between surface-air exchange flux, ENSO and volcanic activity

The mechanistic links between ENSO, volcanic activity and the CO_2 budget occur through the total (land plus ocean) surface-air exchange flux $F_S = C'_a - F_E$, rather than through C'_a. Therefore we examine lagged correlations between F_S (rather than C'_a) and ENSO and volcanic indices. The lagged correlation between time series $X(t)$ and $Y(t)$ is

$$\mathrm{Corr}_{[X,Y]}(\tau) = \langle X(t)Y(t+\tau)\rangle/(\sigma_X\sigma_Y) \quad (4)$$

where τ is the time lag, $\langle\bullet\rangle$ denotes an average over time t, and σ_X and σ_Y are the standard deviations of X and Y.

Lagged correlations between the five ENSO indices and F_S (Fig. 2, left) confirm the well-known relationship (Keeling and Revelle, 1985, Keeling et al., 1995, Jones and Cox, 2005) between ENSO and CO_2 growth rate. Peak correlations between ENSO and F_S (using C'_a at MLO) depend on the choice of ENSO index, ranging between 0.62 for Niño3 and 0.45 for Niño4. The peak correlation is positive (so positive ENSO index anomalies, corresponding with dry, warm El-Niño events, are associated with positive anomalies in F_S or negative anomalies in the total sink $-F_S$). The peak occurs when F_S lags the ENSO index by 3±1 months.

To include the influences of both ENSO and volcanic activity on CO_2 fluxes and growth rate, we define an ENSO-Volcanic Index (EVI) as the linear combination

$$\mathrm{EVI}\,(t) = \mathrm{ENSOI}\,(t-\tau) + \lambda\mathrm{VAI}\,(t) \quad (5)$$

where ENSOI is an ENSO index normalised to zero mean and unit variance; VAI is the global Volcanic Aerosol Index, a measure of volcanically-induced aerosol optical

depth (Ammann et al., 2003); λ is the weight for VAI relative to ENSOI; and τ is the ENSO lag time, a measure of the time for ENSO to affect the CO_2 exchange flux F_S. It is assumed that the VAI affects F_S without time lag. Five alternative versions of the EVI are obtained, corresponding to the five ENSO indices. The EVI depends on two parameters, λ and τ, both of which are well constrained. From Fig. 2 (left) we used τ=3 months for all ENSO indices, so that the maximum correlation between EVI and F_S occurs near t=0. The weight λ was chosen so that the EVI explains as much as possible of F_S, which occurs when λ takes the value maximising the correlation between EVI and F_S. For all five EVI this is close to $\lambda = -16$, the value used hereafter.

Use of the EVI in place of an ENSO index increases the peak correlations with F_S substantially (Fig. 2, right). With F_S calculated from C'_a at MLO and an EVI defined from Niño3, the peak correlation is 0.75. Figure 3 compares peak correlations between the ENSO indices and F_S, and between the corresponding EVI and F_S, using C'_a at both MLO and SPO. Correlations are slightly lower at SPO than MLO, but are still increased by using the EVI rather than corresponding ENSO index. Since λ is negative, a positive anomaly in the VAI component of the EVI is associated with a positive anomaly in the sink $-F_S$ (while a positive anomaly in the ENSO component is associated with negative anomaly in $-F_S$ as noted above).

4 Interdecadal trends in CO_2 airborne fraction

4.1 Initial trend estimate

The total airborne fraction ($a_E = C'_a/F_E = 1 + F_S/F_E$) provides a measure of the relationship between total CO_2 emissions and sinks. We estimated trends in monthly series of a_E inferred from C'_a records from 1959 to 2006. Since a_E is inherently globally aggregated, it is necessary to use estimates of a globally-averaged C'_a. Two estimates were used (see Sect. 2 and Appendix A): from the average of the MLO and SPO CO_2 series with annual cycle removed (denoted GLA), and from a globally-averaged CO_2

series available from 1980 onward, augmented with MLO data before 1980 (denoted GLB).

The trend in a_E was estimated using a stochastic method which accounts for temporal correlation in the time series (see Appendix C for details). The trend is expressed here as a proportional growth rate, defined for a time series $X(t)$ as $r(X) = X'/X$, with units $\%\,y^{-1}$.

The GLA series for 1959–2006 yielded a mean a_E of 0.43 and a proportional growth rate $r(a_E)$=0.24%y^{-1} (with 5% and 95% confidence limits −0.18 and 0.64%\,y^{-1} and probability P=0.81 of a positive trend). The result from the GLB series was nearly identical. This result does not provide an unambiguous, statistically robust determination of the trend in a_E.

4.2 Noise reduction

Detection of trends in a_E can be improved in statistical significance by removing the interannually varying component which is causally linked with ENSO and volcanic activity, using the EVI.

We write an arbitrary time series $X(t)$ as the sum of trend (X^T), mean-annual-cycle (X^C) and anomaly (X^A) components: $X = X^T + X^C + X^A$. The anomaly component is further split as $X^A = X^E + X^U$, where X^U is a noise component uncorrelated with the EVI and X^E is linearly dependent on the EVI. This component is $X^E(t) = \mu \mathrm{EVI}^A(t)$, where μ is the sensitivity of X to the EVI, and use of the anomaly component EVI^A ensures that $X^E(t)$ has zero mean, no trend and no annual cycle. The full decomposition is thus

$$X = X^T + X^C + \mu \mathrm{EVI}^A + X^U \tag{6}$$

When X is a time series over N monthly time points t_n (n=1,...,N), the components are given algorithmically by:

$$X^T(t_n) = P(t_n)$$

$$X^F(t_n) = X(t_n) - X^T(t_n)$$
$$X^C(t_n) = \left\langle X^F(t_m) | \bmod(n, 12) = m \right\rangle$$
$$X^A(t_n) = X^F(t_n) - X^C(t_n) \quad (7)$$

where the trend is defined by fitting a polynomial P to $X(t_n)$, $\langle\bullet\rangle$ denotes an average over the record, and $<\bullet|\text{condition}>$ denotes a conditional average.

The noise-reduced version of $X(t)$, denoted with a superscript (n), is given by subtracting out the externally-forced components X^C and $X^E = \mu \text{EVI}^A$:

$$X^{(n)}(t) = X(t) - X^C(t) - \mu \text{EVI}^A(t) = X^T(t) + X^U(t) \quad (8)$$

The trends of the noise-reduced and original series are identical because the components removed have zero mean and no trend, but the variability of the new series is lower, improving the statistical significance of trends.

This decomposition was applied to the CO_2 sink F_S, yielding noise-reduced series $F_S^{(n)}$, $C_a'^{(n)} = F_E - F_S^{(n)}$ and airborne fraction $a_E^{(n)} = C_a'^{(n)}/F_E$. The sensitivity μ was chosen to minimise the variance of $F_S^U = F_S^A - \mu \text{EVI}^A$, thus placing as much as possible of the anomaly F_S^A into the EVI-correlated component. With lowpass-filtered series F_S and EVI, using an EVI defined from Niño3, the resulting sensitivity is $\mu = 0.9$.

With noise reduction, the GLA series for 1959–2006 yielded a proportional growth rate in total airborne fraction, $r(a_E{}^{(n)})$, of 0.24% y^{-1} (5% and 95% confidence limits −0.04 and 0.50% y^{-1}; probability P=0.92 of a positive trend), around a mean $a_E^{(n)}$ of 0.43. The result with the GLB series is similar but with a slightly lower P of 0.88. Noise reduction therefore does not change the mean result from the above initial trend estimate but provides improved statistical reliability, raising P from 0.81 to about 0.9. This more complete analysis with multiple CO_2 series confirms our earlier result (Canadell et al., 2007) which was derived from the GLB series.

4.3 Uncertainties and implications

The most uncertain quantity affecting the growth rate $r(a_E)$ is F_{LUC}, for which the current best estimate is $F_{LUC} \approx 1.5 \pm 0.5\,PgC\,y^{-1}$ for 2000–2006 (Canadell et al., 2007). Our observed trend in a_E changes from positive to negative if F_{LUC} is reduced to 40% or less of the best estimate, that is, to $0.6\,PgC\,y^{-1}$ or less for 2000–2006 with equivalent proportional reductions in earlier years. However, such a large reduction is well outside the present uncertainty range for F_{LUC}.

We also determined the trend in the apparent airborne fraction (a_{Foss}), even though a_E is the more fundamental carbon-cycle attribute for reasons given in Sect. 2. The proportional growth rate of a_{Foss} for 1959–2006 is small and negative, with $r(a_{Foss}) \approx -0.2 \pm 0.2\%\,y^{-1}$ around a mean of 0.57. The different trends in a_E and a_{Foss} are easily understandable by noting that $r(a_{Foss})$ is the sum of $r(a_E)$ and the growth rate $r(a_{Foss}/a_E)$ in the ratio of the two airborne fractions. This ratio, $a_{Foss}/a_E = 1 + F_{LUC}/F_{Foss}$, decreased fairly steadily through 1959–2006 at a rate $r(a_{Foss}/a_E) \approx -0.4\,\%\,y^{-1}$ (around an average a_{Foss}/a_E of 1.32) because F_{Foss} grew more quickly than F_{LUC} (Canadell et al., 2007). The decreasing trend in F_{LUC}/F_{Foss} therefore accounts fully for the observed different signs in the growth rates of a_{Foss} and a_E.

Two further methodological checks were applied to all estimates of airborne-fraction growth rates. First, estimates of growth rates like $r(a_E)$ were found to have some sensitivity to the exact starting and ending times of the CO_2 series used to determine C'_a. The extent of this sensitivity was investigated with an enhanced stochastic trend estimation method, in which bootstrap subsampling of the time series under test was used to reduce sensitivity to starting and ending times (see Appendix C for details). Results from this method were statistically consistent with those given above, confirming the robustness of the estimated trends.

Second, the entire analysis was also carried out using individual-station CO_2 series from MLO and SPO instead of the globally-averaged series GLA and GLB. Results

were similar to those with the globally-averaged series, despite the fact that $[CO_2]$ at MLO was higher than at SPO by an offset which increased from ∼1 ppm in the 1960s to ∼3 ppm in 2000–2005. By using an exponential-growth model for C_a it can be shown that this offset accounts for a statistically insignificant difference in $r(a_E)$ of about 0.06% y^{-1}.

The result that total airborne fraction increased over 1959–2006 implies that total sinks increased slower than total emissions. Using Eq. (1) to write the relationship between the growth rate $-r(F_S)$ of total sinks ($-F_S$) and the growth rate $r(F_E)$ of total emissions, we obtain:

$$-r(F_S) = r(F_E) - \left(\frac{a_E}{1-a_E}\right) r(a_E) \quad (9)$$

$$1.6\,(\pm 0.2) \quad 1.8\,(\pm <0.1) \quad -0.2\,(\pm 0.2)$$

The numbers beneath each term give average values in % y^{-1} for 1959–2006. Both total sinks and total emissions grew significantly, but the observation of an increasing airborne fraction shows that sinks grew slightly slower than emissions. Use of the observed atmospheric CO_2 budget to partition the sinks into land and ocean components shows that the ocean fraction of the total sinks decreased substantially whereas the land fraction did not (Canadell et al., 2007).

The observed increase in the airborne fraction is in not in agreement with available predictions of coupled carbon-climate models. The average prediction of 11 models (Friedlingstein et al., 2006) for 1959–2006 is a decrease in a_E at $-0.27 \pm 0.36\%\,y^{-1}$, suggesting that these models tend to overestimate the rate of increase in total sinks as CO_2 concentrations rise. Equation (9) shows that this is a sensitive test for carbon-climate model predictions of trends in total sinks, because the sign of $r(a_E)$ is determined by the small difference between the two larger quantities $r(F_E)$ and $-r(F_S)$.

5 Unified assessment of the drivers of CO_2 growth

To assess the relative effects on CO_2 growth of changes in airborne fraction and anthropogenic drivers of CO_2 emissions, we use an extended form of the Kaya identity. In its usual form (Nakicenovic et al., 2000, Nakicenovic, 2004, Raupach et al., 2007), the Kaya identity expresses global fossil-fuel CO_2 emissions as $F_{Foss} = Pgef$, where P is global population, $g = G/P$ is per capita income or per capita GDP, $e = E/G$ is the energy intensity of GDP, $f = F_{Foss}/E$ is the fossil-carbon intensity of energy, G is global GDP-PPP, and E is global primary energy consumption. An equivalent expression is $F_{Foss} = Pgh_{Foss}$, where $h_{Foss} = F_{Foss}/G = ef$ is the fossil-fuel carbon intensity of the global economy.

We modify this identity in two ways, first to describe total emissions ($F_E = F_{Foss} + F_{LUC}$) rather than F_{Foss}. Land use change emissions can be written in Kaya form as $F_{LUC} = Pgh_{LUC}$, where $h_{LUC} = F_{LUC}/G$ is the land-use-change carbon intensity of the global economy, corresponding to h_{Foss} above. The Kaya identity for total CO_2 emissions is then

$$F_E = Pgh_{Foss} + Pgh_{LUC} = Pgh_E \tag{10}$$

where $h_E = F_E/G = h_{Foss} + h_{LUC}$ is the total carbon intensity of the global economy, accounting for both fossil fuels and land use change. Second, we describe the atmospheric CO_2 growth rate (C'_a) by introducing the airborne fraction $a_E = C'_a/F_E$ into Eq. (10). The end result after both these changes is an extended Kaya identity in which a_E appears as an extra factor:

$$C'_a = Pgh_E a_E \tag{11}$$

The proportional growth rates of factors in Eqs. (10) and (11) are related by

$$r(F_E) = r(P) + r(g) + r(h_E)$$
$$r(C'_a) = r(P) + r(g) + r(h_E) + r(a_E) \tag{12}$$

because $r(X) = X'/X$ yields $r(XYZ) = r(X) + r(Y) + r(Z)$ for any X, Y and Z. All terms in Eq. (12) have units time^{-1}. Note that $r(C_a') = C_a''/C_a'$ is the proportional growth rate of the CO_2 growth rate, a measure of the second derivative of C_a.

Figures 4a and b respectively show time series of the factors in the Kaya identity for F_E, (Eq. 10) and the extended Kaya identity for C_a' (Eq. 11) for the period 1959–2006, with series are normalised to 1 in 1980 so that trends can be compared. Figures 5a and b show the corresponding proportional growth rates (Eq. 12), with 7-year smoothing for clarity. Average growth rates of all factors, with 5% to 95% confidence intervals, are given in Table 1.

For F_E (Figs. 4a and 5a) the average growth rate $r(F_E)$ over 1959–2006 was 1.8% y^{-1}, with interannual variability from less than 0.5 to over 3% y^{-1}. This growth was driven by additive contributions of +1.7% y^{-1} from $r(P)$ (growth in population), +1.8% y^{-1} from $r(g)$ (growth in income), and −1.7% y^{-1} from $r(h_E)$ (reduction or improvement in the total carbon intensity of the global economy). Uncertainties in all these growth rates are low (0.1% y^{-1} or less; Table 1).

The CO_2 growth rate C_a' (Fig. 4b) is noisy, because of the interannual variability discussed above. Over the last five decades C_a' increased inexorably, reaching an average of $C_a' \approx 4.1 \pm 0.1$ PgC y^{-1} or $[CO_2]' = 1.9$ ppm y^{-1} through 2000–2006 (Canadell et al., 2007). The drivers of this increase can be expressed (Fig. 5b and Eq. (12) as contributions from the growth rates $r(P)$, $r(g)$, $r(h_E)$ and $r(a_E)$ to $r(C_a') = C_a''/C_a'$, the growth rate of the CO_2 growth rate. Even with the 7-year smoothing used here, $r(C_a')$ fluctuated strongly around a mean of +1.9% y^{-1}, with contributions from $r(P)$, $r(g)$, $r(h_E)$ and $r(a_E)$ given in Table 1.

6 Discussion and conclusions

There were significant interdecadal trends in the emissions drivers P, g and h_E through 1959–2006 (Fig. 5a and Table 1). Growth in population (P) slowed from 2 to 1.2% y^{-1}.

Per capita income (g) grew more rapidly since 2000 than over the previous four decades, with $r(g)$=3.0% y^{-1} over 2000–2006 compared with 1.8% y^{-1} over 1959–1999. Also, the negative growth rate (improvement) in the carbon intensity of the economy (h_E) declined since 2000: $r(h_E)$ was −1.2% y^{-1} over 2000–2006, compared with a mean of −1.7% y^{-1} over 1959–1999. (Figures for $r(h_E)$ differ from Canadell et al., 2007 for two reasons: the use of GDP-PPP here and GDP-MER (Market Exchange Rate) there, and the inclusion of F_{LUC} in h_E here).

As noted elsewhere (Raupach et al., 2007, Canadell et al., 2007), these trends have together driven a substantial recent increase in the growth rate of total emissions, with $r(F_E)$=3.0% y^{-1} over 2000–2006 compared with 1.9% y^{-1} over 1959–1999. The growth rate in F_E ($= F_{Foss} + F_{LUC}$) is slightly lower than the recent growth rate in fossil-fuel emissions ($r(F_{Foss})$=3.3% y^{-1} over 2000–2006) because there has been no recent growth in the land-use-change emission (F_{LUC}).

Similar trends appear in the growth rate of the CO_2 growth rate, $r(C'_a) = C''_a/C'_a$ (Fig. 5b and Table 1). Averaged over the whole period 1959–2006, most of the interdecadal trend ($r(C'_a) \approx 1.9\%\, y^{-1}$) was attributable to increasing emissions ($r(F_E) \approx 1.8\%\, y^{-1}$), caused in turn by the growth rates of P, g and h_E. A small component of $r(C_a{}')$, about 0.2% y^{-1} out of 1.9% y^{-1}, was caused by the interdecadal growth in airborne fraction, $r(a_E)$ (these figures do not satisfy Eq. (12) exactly because of statistical uncertainties and roundoff errors).

Most of the strong interannual variability in $r(C'_a)$) originates from variability in the CO_2 exchange flux F_S and thence the airborne-fraction term in Eq. (11). Much of this variability in turn is associated with the EVI. Subtracting the EVI-correlated fluctuating component out of C'_a and a_E as in Sect. 4.2, we obtain a noise-reduced form of the extended Kaya identity, $C'^{(n)}_a = Pgh_E a^{(n)}_E$. Figure 5c shows the growth rates of extended Kaya factors with this noise reduction. The variability in each of $r(C_a{}'^{(n)})$ and $r(a^{(n)}_E)$ is about half of the equivalent variability without noise reduction (Fig. 5b).

The extended Kaya identity allows estimation of the relative impacts on future [CO_2]

of likely trends in airborne fraction and the drivers of total emissions (P, g and h_E). To do this we consider the time interval Δt_x to reach a specified future concentration $[CO_2]_x$ at a given $r(C_a{}')$ (the growth rate of the CO_2 growth rate). The interval Δt_x can be determined analytically (Appendix D). We take $[CO_2]_x$=450 ppm and initial conditions $[CO_2]$=383 ppm and $[CO_2]'$=2 ppm y^{-1} in 2008. If $r(C'_a)$ continues at 2.0% y^{-1} (approximately the average for 1959–2006), then $[CO_2]$ will reach 450 ppm in 26 years, in 2034. An increase in $r(C'_a)$ of 1% y^{-1}, by any mechanism, shortens the time to reach 450 ppm by about 2.6 years. Since 2000, the combination of influences from the emissions drivers P, g and h_E have indeed increased $r(C'_a)$ by more than 1% y^{-1}, as discussed above. For future growth in airborne fraction to have a comparable influence, $r(a_E)$ would need to increase several-fold from its 1959–2006 average of 0.2% y^{-1}.

To reduce emissions and thence atmospheric CO_2, it is necessary to reduce the growth rates of the emissions drivers P, g and h_E in some combination. Growth in population (P) is presently just over 1% y^{-1} and is forecast to decline to zero in the second half of the 21st century (Lutz et al., 2001). Growth in global per capita income (g) is needed to improve quality of life in the developing world. This leaves the primary option as increasing the negative growth rate in carbon intensity (h_E). To achieve a reduction rate in total emissions of −2% y^{-1} (which would halve emissions in 35 years) in the presence of global growth rates of 2% y^{-1} in g and 1% y^{-1} in P, it is necessary to achieve a decline in h_E at a rate of around −5% y^{-1}, three times the 1959–2006 average. This highlights the significance of recent trends in emissions and carbon intensity.

Appendix A

Data sources and treatments

A1 CO_2 concentrations and growth rates

Four monthly CO_2 time series were used, denoted MLO, SPO, GLA and GLB. The first two were monthly time series for baseline [CO_2] at Mauna Loa (MLO, commencing March 1958) and the South Pole (SPO, commencing June 1957) from the Scripps Institution of Oceanography http://scrippsco2.ucsd.edu/data/data.html (Keeling et al., 2001, 2005). The versions of these series used here were gap-filled and had the quasi-regular seasonal cycle removed by subtraction of a 4-harmonic fit with a linear gain factor. The monthly CO_2 growth rate with seasonal cycle removed was calculated from each series by a centred first difference. The third and fourth series were estimates of a globally averaged CO_2. The GLA series was formed from the average of MLO and SPO. The GLB series consisted of a globally-averaged CO_2 series available from January 1980 onward, augmented with MLO data for 1958–1979, with both series from the Earth Systems Research Laboratory of the National Oceanographic and Atmospheric Administration (NOAA-ESRL) http://www.esrl.noaa.gov/gmd/ccgg/trends/. The GLB series includes the annual cycle. Its trend is smooth but there is a discontinuity in the annual cycle at the join in 1980. The annual cycle was removed for determination of the trend in a_E.

A2 CO_2 emissions

The emissions datasets are identical to those in Canadell et al. (2007) and Raupach et al. (2007). Annual data on F_{Foss} to 2004 are from the CDIAC (Marland and Rotty, 1984, Marland et al., 2006) http://cdiac.esd.ornl.gov/trends/emis/em_cont.htm, augmented by estimates for 2005 and 2006. Data on F_{LUC} are from Houghton (1999, 2003). A monthly series for $F_E = F_{\mathrm{Foss}} + F_{\mathrm{LUC}}$ for 1958 onward was constructed by spline interpolation

of annual series for F_{Foss} and F_{LUC}. It is likely that there are repeating annual cycles in both F_{Foss} and F_{LUC} caused by seasonal patterns in energy consumption and land management practices, but interpolation of annual data gives a good approximation to monthly series with the annual cycle removed.

A3 ENSO indices

Five ENSO indices were used: Niño3, Niño3.4, Niño4, SOI, from http://www.cpc.ncep.noaa.gov/data/indices/sstoi.indices, and the MEI, from http://www.cdc.noaa.gov/ClimateIndices/List/. The MEI is constructed from the first principal components of sea-level pressure, zonal and meridional components of the surface wind, sea surface temperature, surface air temperature, and total sky cloudiness fraction (Wolter and Timlin, 1993, 1998).

A4 Volcanic aerosol index

VAI data in latitude bands (Ammann et al., 2003), to 1998, were obtained from ftp://ftp.ncdc.noaa.gov/pub/data/paleo/climate_forcing/volcanic_aerosols/ammann2003b_volcanics.txt. A global VAI was calculated by averaging with area weighting. The data were extended to 2006 assuming no volcanic activity between 1998 and 2006, consistent with Mishchenko et al. (2007).

A5 GDP-PPP and population

For 1970 and later, data sources are identical to those in Raupach et al. (2007). Global population (P) was from the United Nations Statistics Division http://unstats.un.org/unsd/snaama/selectionbasicFast.asp. Global GDP-PPP (G) was from the World Economic Outlook of the International Monetary Fund http://www.imf.org/external/pubs/ft/weo/2006/02/data/download.aspx. For times before 1970, both P and G were obtained from "Historical Statistics for the World Economy: 1-2003 AD" by Angus Maddison

http://www.ggdc.net/maddison/. There was good agreement between these datasets in the overlap period 1970–2003.

Appendix B

Time series analysis

B1 Normalised cumulative spectra and cospectra

Let $X(t)$ and $Y(t)$ be continuous processes in time, or discrete time series, with zero mean. The normalised cumulative spectrum $\mathrm{NC}_{[X,X]}(f)$ of $X(t)$ is the integral from 0 to f of the spectrum of the unit-variance process $X(t)/\sigma_X$ (where σ_X is the standard deviation of X); it is the fraction of the variance of X contributed by frequencies less than f. The normalised cumulative cospectrum $\mathrm{NC}_{[X,Y]}(f)$ of $X(t)$ and $Y(t)$ is the integral from 0 to f of the cospectrum of the unit-variance processes $X(t)/\sigma_X$ and $Y(t)/\sigma_Y$; it is the fractional contribution to the XY covariance $\mathrm{Cov}_{[X,Y]}$ from frequencies less than f, normalised so that $\mathrm{NC}_{[X,Y]}(f)$ approaches the correlation coefficient $\mathrm{Cov}_{[X,Y]}/(\sigma_X\sigma_Y)$ as $f \to \infty$.

B2 Fourier-transform lowpass filtering

The lowpass-filtered version of a series $X(t)$ was obtained by (a) taking the Fourier transform of $X(t)$; (b) setting Fourier components above the lowpass cutoff frequency to zero; (c) taking the inverse Fourier transform.

Appendix C

Trend estimation

The trend of a series $X(t)$ was estimated using a stochastic method as in (Le Quere et al., 2007) and (Canadell et al., 2007), accounting for temporal correlation between data points. First, the trend X^T was found by conventional least-squares regression, yielding a trend line $X^T = x_0 + x_1 t$. The lagged autocorrelation function of the residual $(X - X^T)$ was fitted with an autoregressive (AR) model (Box et al., 1994) and used to generate an ensemble of 1000 stochastic realisations of the data with mean trend X^T and residuals correlated as in the data itself. The probability density function (PDF) of the slopes (x_1) in this ensemble was calculated, yielding trend statistics.

For supplementary investigation of the sensitivity of trends to the start and end points of the series $X(t)$, an "enhanced stochastic" method was used. This extends the stochastic method by taking the slope of the trend line X^T to be the mean of a 1000-member ensemble obtained by "bootstrap" (with replacement) sampling of sub-series of $X(t)$ with random starting and stopping times (t_0, t_1), such that $(t_1 - t_0)$ is at least a minimum fraction $f_{\min}$ of the total duration of the data series $X(t)$. We took $f_{\min} = 0.8$. The statistics of this ensemble are similar to those of the original series $X(t)$, with sensitivity to choice of t_0 and t_1 reduced by averaging over many realisations.

Appendix D

Time to reach a specified CO_2 concentration

We seek the time interval Δt_x to reach a specified future concentration $[CO_2]_x$, with a given steady growth rate of the CO_2 growth rate, $r_C = r(C'_a)$, and given initial concentration $[CO_2]_0$ and rate of increase $[CO_2]'_0$ at time t_0. Thus $r_C = [CO_2]''_0/[CO_2]'_0$, and is

held steady. The equation governing $[CO_2](t)$ is

$$[CO_2]'' = r_C [CO_2]' \quad \text{(D1)}$$

and the resulting CO_2 trajectory is

$$[CO_2](t) = [CO_2]_0 + + \frac{[CO_2]'_0}{r_C} \exp\left((r_C(t - t_0) - 1\right) \quad \text{(D2)}$$

At a given r_C, the time to reach $[CO_2]_x$ is

$$\Delta t_x = \frac{1}{r_C} \ln\left(r_C T - 1\right) \quad \text{(D3)}$$

where $T = ([CO_2]_x - [CO_2]_0)/[CO_2]'_0$ is a time scale. Physically, T is the time to reach $[CO_2]_x$ when the rate of increase in $[CO_2]$ is held steady at its initial value $[CO_2]'_0$. If $r_C > 0$, then Δt_x is less than T. In the limit $r_C \to 0$, Δt_x approaches T.

Acknowledgements. This work was undertaken by the Global Carbon Project (GCP, www.globalcarbonproject.org) of the Earth System Science Partnership (www.essp.org). Support for the GCP from the Australian Climate Change Science Program is acknowledged with appreciation. We gratefully acknowledge the teams from both the Scripps Institution of Oceanography and NOAA-ESRL, who have publicly released the CO_2 records without which this work would not have been possible. We thank P. Briggs for help with preparation of figures.

References

Ammann, C. M., Meehl, G. A., Washington, W. M., and Zender, C. S.: A monthly and latitudinally varying volcanic forcing dataset in simulations of 20th century climate, Geophys. Res. Lett., 30, 1657, doi:10.1029/2003GL016875, 2003.

Box, G., Jenkins, G. M., and Reinsel, G.: Time series analysis: forecasting and control, 3rd edition, Prentice Hall, Englewood Cliffs, NJ, USA, 592 pp., 1994.

Canadell, J. G., Le Quere, C., Raupach, M. R., Field, C. B., Buitenhuis, E. T., Ciais, P., Conway, T. J., Gillett, N. P., Houghton, R. A., and Marland, G.: Contributions to accelerating atmospheric CO_2 growth from economic activity, carbon intensity, and efficiency of natural sinks, *PNAS*, 0702737104, 2007.

Enting, I. G.: Laplace transform analysis of the carbon cycle, Environ. Model. Software, 22, 1488–1497, 2007.

Friedlingstein, P., Cox, P., Betts, R., Bopp, L., von Bloh, W., Brovkin, V., Cadule, P., Doney, S., Eby, M., Fung, I., Bala, G., John, J., Jones, C., Joos, F., Kato, T., Kawamiya, M., Knorr, W., Lindsay, K., Matthews, H. D., Raddatz, T., Rayner, P., Reick, C., Roeckner, E., Schnitzler, K. G., Schnur, R., Strassmann, K., Weaver, A. J., Yoshikawa, C., and Zeng, N.: Climate-carbon cycle feedback analysis: Results from the C4MIP model intercomparison, J. Climate, 19, 3337–3353, 2006.

Gruber, N., Friedlingstein, P., Field, C. B., Valentini, R., Heimann, M., Richey, J. D., Romero Lankao, P., Schulze, E.-D., and Chen, C.-T. A.: The vulnerability of the carbon cycle in the 21st century: an assessment of carbon-climate-human interactions, in: The Global Carbon Cycle: integrating humans, climate, and the natural world, edited by: Field, C. B. and Raupach, M. R., Island Press, Washington, USA, 45–76, 2004.

Gu, L. H., Baldocchi, D. D., Wofsy, S. C., Munger, J. W., Michalsky, J. J., Urbanski, S. P., and Boden, T. A.: Response of a deciduous forest to the Mount Pinatubo eruption: enhanced photosynthesis, Science, 299, 2035–2038, 2003.

Houghton, R. A.: The annual net flux of carbon to the atmosphere from changes in land use 1850–1990, Tellus B, 51, 298–313, 1999.

Houghton, R. A.: Why are estimates of the terrestrial carbon balance so different?, Global Change Biol., 9, 500–509, 2003.

Jones, C. D., Collins, M., Cox, P. M., and Spall, S. A.: The carbon cycle response to ENSO: a coupled climate-carbon cycle model study, J. Climate, 14, 4113–4129, 2001.

Jones, C. D. and Cox, P. M.: Modeling the volcanic signal in the atmospheric CO2 record, Global Biogeochem. Cy., 15, 453-465, 2001.

Jones, C. D. and Cox, P. M.: On the significance of atmospheric CO_2 growth rate anomalies in 2002–2003, Geophys. Res. Lett., 32, L14816, doi:10.1029/2005GL023027, 2005.

Keeling, C. D., Piper, S. C., Bacastow, R. B., Wahlen, M., Whorf, T. P., Heimann, M., and Meijer, H. A.: Exchanges of atmospheric CO_2 and $^{13}CO_2$ with the terrestrial biosphere and oceans from 1978 to 2000: 1. global aspects, SIO Reference Series, 01-06, Scripps Institution of

Oceanography, San Diego, USA, 88, 2001.
Keeling, C. D., Piper, S. C., Bacastow, R. B., Wahlen, M., Whorf, T. P., Heimann, M., and Meijer, H. A.: Atmospheric CO_2 and $^{13}CO_2$ exchange with the terrestrial biosphere and oceans from 1978 to 2000: observations and carbon cycle implications, in: A history of atmospheric CO_2 and its effects on plants, animals, and ecosystems, edited by: Ehleringer, J. R., Cerling, T. E., and Dearing, M. D., Springer Verlag, New York, USA, 83–113, 2005.
Keeling, C. D. and Revelle, R.: Effects of El-Niño southern oscillation on the atmospheric content of carbon-dioxide, Meteoritics, 20, 437–450, 1985.
Keeling, C. D., Whorf, T. P., Wahlen, M., and Vanderplicht, J.: Interannual extremes in the rate of rise of atmospheric carbon-dioxide since 1980, Nature, 375, 666–670, 1995.
Knorr, W., Scholze, M., Gobron, N., Pinty, B., and Kaminski, T.: Global-scale drought caused atmospheric CO_2 increase, EOS, 86, 178–181, 2005.
Le Quere, C., Rodenbeck, C., Buitenhuis, E. T., Conway, T. J., Langenfelds, R., Gomez, A., Labuschagne, C., Ramonet, M., Nakazawa, T., Metzl, N., Gillett, N., and Heimann, M.: Saturation of the southern ocean CO_2 sink due to recent climate change, Science, 316, 1735–1738, 2007.
Lutz, W., Sanderson, W., and Scherbov, S.: The end of world population growth, Nature, 412, 543–545, 2001.
Marland, G., Boden, T. A., and Andres, R. J.: Global, regional, and national CO_2 emissions, in: Trends: a compendium of data on global change, Carbon Dioxide Information Analysis Center, Oak Ridge National Laboratory, US Department of Energy, Oak Ridge, Tennessee, USA, http://cdiac.esd.ornl.gov/trends/emis/em_cont.htm, 2006.
Marland, G. and Rotty, R. M.: Carbon dioxide emissions from fossil fuels: a procedure for estimation and results for 1950–82, Tellus B, 36, 232–261, 1984.
Mishchenko, M. I., Geogdzhayev, I. V., Rossow, W. B., Cairns, B., Carlson, B. E., Lacis, A. A., Liu, L., and Travis, L. D.: Long-term satellite record reveals likely recent aerosol trend, Science, 315, 1543, 2007.
Nakicenovic, N.: Socioeconomic driving forces of emissions scenarios, in: The Global Carbon Cycle: integrating humans, climate, and the natural world, edited by: Field, C. B. and Raupach, M. R., Island Press, Washington, 225–239, 2004.
Nakicenovic, N., Alcamo, J., Davis, G., de Vries, B., Fenhann, J., Gaffin, S., Gregory, K., Grubler, A., Jung, T. Y., Kram, T., La Rovere, E. L., Michaelis, L., Mori, S., Morita, T., Pepper, W., Pitcher, H., Price, L., Raihi, K., Roehrl, A., Rogner, H.-H., Sankovski, A., Schlesinger,

M., Shukla, P., Smith, S., Swart, R., van Rooijen, S., Victor, N., and Dadi, Z.: IPCC Special Report on Emissions Scenarios, Cambridge University Press, Cambridge, UK, and New York, USA, 599 pp., 2000.

Oeschger, H., Siegenthaler, U., and Heimann, M.: The carbon cycle and its perturbations by man, in: Interactions of Energy and Climate, edited by: Bach, W., Pankrath, J., and Williams, J., Reidel, Dordrecht, The Netherlands, 107–127, 1980.

Raupach, M. R., Marland, G., Ciais, P., Le Quere, C., Canadell, J. G., Klepper, G., and Field, C. B.: Global and regional drivers of accelerating CO_2 emissions, PNAS, 0700609104, 2007.

Sabine, C. L., Heimann, M., Artaxo, P., Bakker, D. C. E., Chen, C.-T. A., Field, C. B., Gruber, N., Le Quere, C., Prinn, R. G., Richey, J. D., Romero Lankao, P., Sathaye, J. A., and Valentini, R.: Current status and past trends of the global carbon cycle, in: The global carbon cycle: integrating humans, climate, and the natural world, edited by: Field, C. B. and Raupach, M. R., Island Press, Washington, USA, 17–44, 2004.

Wolter, K. and Timlin, M. S.: Monitoring ENSO in COADS with a seasonally adjusted principal component index, in: Proceedings of the 17th Climate Diagnostics Workshop, Oklahoma Climatological Survey, Cooperative Institute for Mesoscale Meteorological Studies, and the School of Meteorology, University of Oklahoma, Norman, OK, USA, 52–57, 1993.

Wolter, K. and Timlin, M. S.: Measuring the strength of ENSO – how does 1997/98 rank?, Weather, 53, 315–324, 1998.

Zeng, N., Mariotti, A., and Wetzel, P.: Terrestrial mechanisms of interannual CO_2 variability, Global Biogeochem. Cy., 19, GB1016, doi:10.1029/2004GB002273, 2005.

Table 1. Proportional growth rates ($r(X) = X'/X$, in % y^{-1}) of factors in the Kaya identity ($F_E = Pgh_E$) and the extended Kaya identity ($C'_a = Pgh_E a_E$), for periods 1959–2006, 1959–1999 and 2000–2006 (inclusive of end years). Errors denote approximate 5% to 95% confidence intervals. Where not shown, errors are less than 0.1% y^{-1}. Roundoff errors are responsible for slight departures from Eq. (12).

Period	1959–2006	1959–1999	2000–2006
$r(F_E)$	1.8	1.9	3.0
$r(P)$	1.7	1.7	1.2
$r(g)$	1.8	1.8	3.1±0.1
$r(h_E)$	−1.7	−1.7	−1.2±0.1
$r(a_E)$	0.2±0.2	0.2±0.3	0.2±2.7
$r(C_a')$	1.9±0.3	1.9±0.4	3.0±2.7

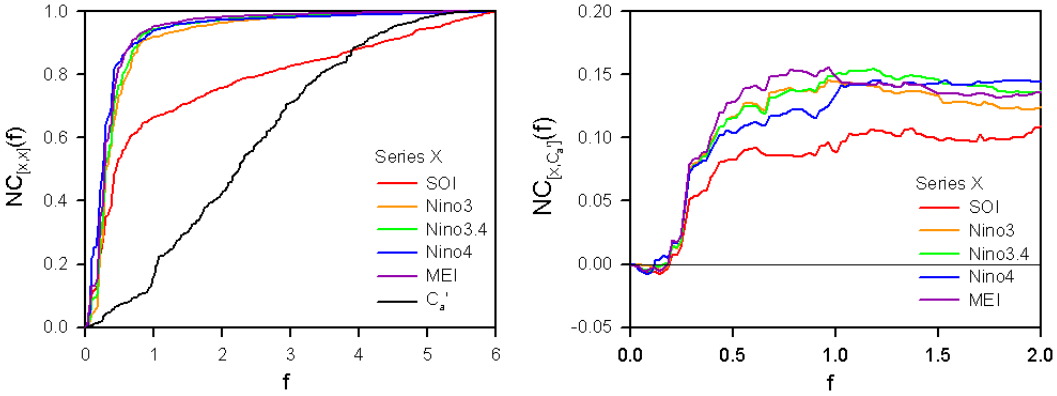

Fig. 1. (Left) normalised cumulative spectra of MLO CO_2 growth rate C'_a (black) and ENSO indices (coloured), showing the total fraction of the variance contributed by frequencies less than f. (Right) normalised cumulative cospectra of C'_a with ENSO indices. Colour code for ENSO indices: SOI (red), Niño3 (orange), Niño3.4 (green), Niño4 (blue), MEI (violet).

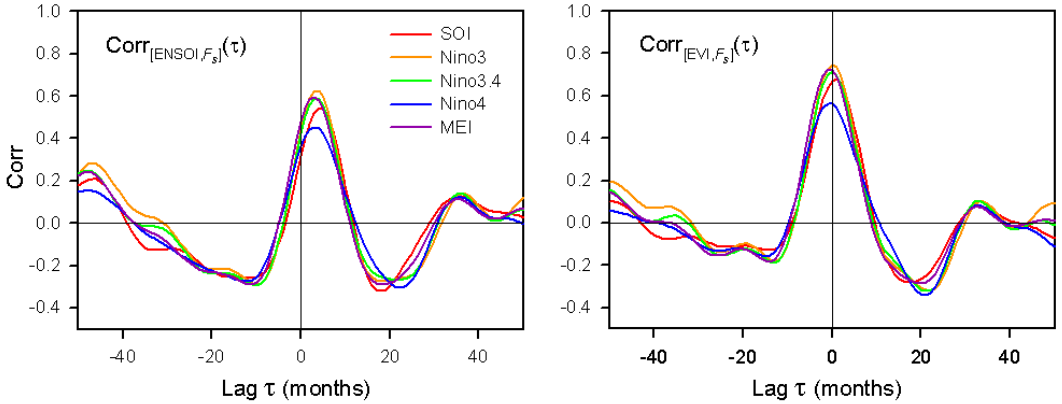

Fig. 2. Lagged cross-correlation functions between (left) ENSO indices and F_S, $\mathrm{Corr}_{[\mathrm{ENSOI},F_S]}(\tau)$, and (right) corresponding ENSO-Volcanic Indices (EVI) and F_S, $\mathrm{Corr}_{[\mathrm{EVI},F_S]}(\tau)$. The surface-air exchange flux $F_S = C'_a - F_E$ was calculated from monthly MLO CO_2 with seasonal cycle removed. All series are lowpass-filtered ($f < 0.8\ \mathrm{y}^{-1}$). Colour code for different ENSO indices and corresponding EVI matches Fig. 1.

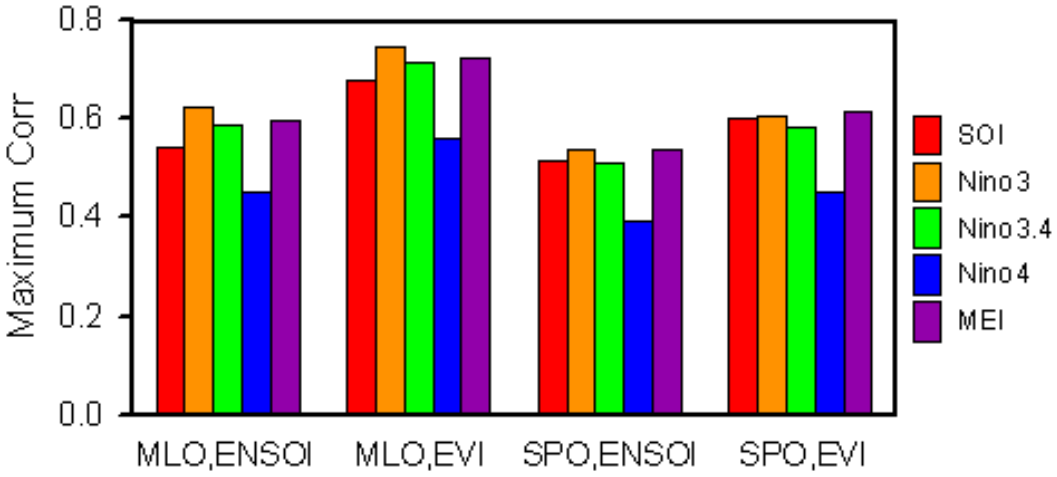

Fig. 3. Maximum lagged correlations between ENSO indices and F_S, and between EVI and F_S, using F_S from CO_2 at MLO and SPO. All series are lowpass-filtered ($f < 0.8\ y^{-1}$). Colour code for different ENSO indices and corresponding EVI matches Fig. 1.

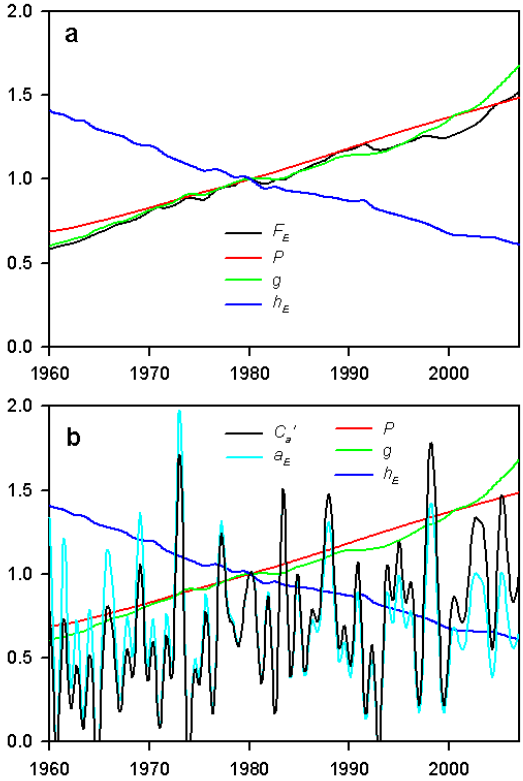

Fig. 4. (a) factors in the Kaya identity, $F_E = Pgh_E$, with F_E (total emissions) in black, P (population) in red, g (per capita GDP-PPP) in green and h_E (carbon intensity of GDP-PPP) in dark blue. **(b)** factors in the extended Kaya identity, $C_a' = Pgh_E a_E$, with C_a' in black, a_E in sky blue and other colours as in left plot. All factors are normalised to 1 in 1980.

BGD
5, 2867–2896, 2008

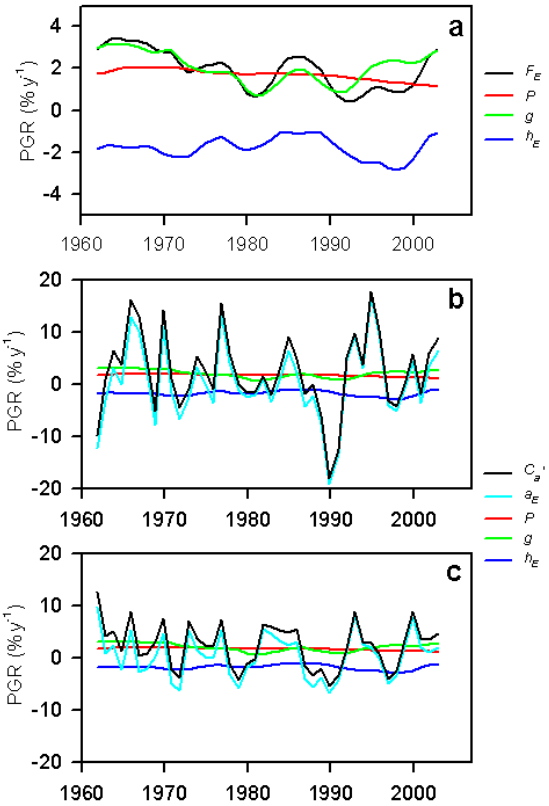

Fig. 5. **(a)** proportional growth rates ($\%\,y^{-1}$) of factors in the Kaya identity, $F_E = Pgh_E$; **(b)** growth rates of factors in the extended Kaya identity, $C_a' = Pgh_E a_E$; **(c)** growth rates of factors in the noise-reduced version of the extended Kaya identity, $C_a'^{(n)} = Pgh_E a_E^{(n)}$, where $((n))$ denotes removal of the EVI-correlated fluctuating component. All growth rates are smoothed with a 7-year running mean. Colours match Fig. 4.